Article

Fermi Level Engineering for Large Permittivity in BaTiO$_3$-Based Multilayers

Christopher Castro Chavarría [1,2,]*, Sandrine Payan [1], Jean-Paul Salvetat [3], Mario Maglione [1] and Andreas Klein [2]

[1] ICMCB, CNRS, Université de Bordeaux, UMR 5026, F-33600 Pessac, France; sandrine.payan@u-bordeaux.fr (S.P.); mario.maglione@u-bordeaux.fr (M.M.)

[2] Department of Materials and Earth Sciences, Electronic Structure of Materials, Technische Universität Darmstadt, Otto-Berndt-Str. 3, 64287 Darmstadt, Germany; andreas.klein@tu-darmstadt.de

[3] PLACAMAT, CNRS, Université de Bordeaux, UMS 3626, F-33600 Pessac, France; jean-paul.salvetat@placamat.cnrs.fr

* Correspondence: christopher.castro-chavarria@u-bordeaux.fr

check for updates

Abstract: Multilayered doped BaTiO$_3$ thin films have been fabricated by physical vapor deposition (PVD) on low-cost polycrystalline substrates with the aim to improve dielectric properties by controlling point charge defects at the interfaces. We show that carefully designed interfaces lead to increasing the relative permittivity of the BaTiO$_3$ thin films, in contradiction with the common belief that interfaces behave as dead layers. High relative permittivity up to 1030 and $\tan\delta = 4\%$ at 100 kHz and room temperature were obtained on BaTiO$_3$ multilayered films deposited on Si/Pt substrates by PVD. The large permittivity is suspected to be an extrinsic contribution due to band bending at the interfaces, as inferred by in-situ X-ray photoelectron spectroscopy. A 20-nm depletion layer was found to be associated with an interdiffusion of dopants, as measured by depth profiling with time-of-flight secondary ion mass spectrometry. The films exhibit high permittivity and low dielectric losses stable between 200 and 400 K, which meet the requirement of electronic applications.

Keywords: thin films; barium titanate; XPS; TOF-SIMS; surface analysis; large permittivity; Fermi level position; interfaces

1. Introduction

Polycrystalline BaTiO$_3$ (BTO) usually loses its main properties when deposited as thin films. Much lower permittivity than in bulk and no clear phase transition are often observed as a result of random internal strain induced by the deposition process, lattice expansion mismatch, or (local) variation of stoichiometry. Deep investigations since the mid-nineties have shown that restoring the polarization and dielectric properties in BaTiO$_3$ (BTO) thin films requires advanced processes. The microstructure of thin films can span from granular as in chemical solution deposited films [1,2] to epitaxial as in Molecular Beam Epitaxy (MBE) [3,4] and Pulsed Laser Deposition (PLD) grown films [5,6] for a large variety of substrates. In many instances, dielectric, polarization and piezoelectric properties may be recovered, sometimes thanks to the substrate-induced stress on the films. Restored dielectric permittivity and losses, however, may suffer from stability issues versus temperature or stress changes, which is detrimental for many applications. The scope of the present paper is to use artificially charged interfaces in BaTiO$_3$ multilayers to stabilize large dielectric permittivity in integrated 300-nm-thick structures deposited on Si/Pt substrates.

Interface control in ferroelectric materials is a long-standing issue needing a deeper understanding, mostly about the interplay between point charge defects and interfaces.

Back in the seventies, donor doping (La, Nb) in BaTiO$_3$ ceramics resulted in spectacular resistance changes, which were modelled using grain boundary band bending [7]. From the mid-nineties, large and extrinsic dielectric permittivities have been reported in a large variety of bulk polycrystalline materials, all explained using space charge or Maxwell–Wagner models [8–11] without microscopic insight into the actual interfaces. Here, to achieve interface control, we have combined charged point defect substitution (Mn, Nb, La) in BaTiO$_3$ thin films and multilayer architectures. We first show that the Fermi level in individual films may be tuned from very close to the conduction band in reduced (V$_O$) or donor-doped films (La, Nb) to the mid-gap under acceptor-doping (Mn). Stacking these films induced band bending over more than 10 nm in La/Nb and in Mn/Nb stacks as evidenced by X-ray photoelectron spectroscopy, which was performed in situ along stepwise interface formation. In the case of La/Nb interfaces this unusual band bending induced large dielectric permittivity of more than 1000 together with moderate losses of less than 5% and temperature stability over more than 100 K. We then linked these appealing dielectric parameters and band bending to cross-diffusion of dopants between the layers. This cross-diffusion has been directly evidenced by time-of-flight secondary ion mass spectroscopy (TOF-SIMS) depth profiling. The cross-diffusion takes place over more than 10 nm in the case of Nb and La, which is very large. These heterostructures are one example of how band bending and free charge accumulation can artificially increase the effective dielectric permittivity while moderating dielectric losses and leakage currents. Unlike polycrystalline bulk materials, multilayers offer an efficient platform for understanding the origin of artificially enhanced permittivity using in situ X-ray photoelectron spectroscopy (XPS) and TOF-SIMS on the same samples.

2. Materials and Methods

Films were deposited by magnetron sputtering from home-made targets including the required amount of dopants. Target compositions as well as sputtering conditions are reported in Table 1. We used sputtering parameters and chambers as reported in our former investigations [12–14]. The different multilayers were deposited as 3 layers alternating between Mn-, Nb- or La-doped BaTiO$_3$. We chose 5, 10 and 20 nm of Mn- or La-doped layers as top and bottom layers and 290, 280 and 260 nm of an Nb core layer, respectively, hence conserving a total thickness of 300 nm for each sample. In doing so, we expected that properties would not vary between the different stacks if only interfaces play a significant role. These heterostructures will be referred to as MNM5, MNM10 and MNM20. With the same approach, samples NMN20, LNL10 and NLN10 are heterostructures alternating between Nb (N), Mn (M) and La (L) with the thickness of the top and bottom layers at the end, always conserving a total of 300 nm (e.g., LNL10, is a sample with a 10-nm La bottom layer, a 280-nm Nb core layer and a 10-nm La top layer).

Table 1. Physical vapor deposition (PVD) sputtering conditions for (un) doped BaTiO$_3$ (BTO) thin films and doping concentration of targets.

Sputtering Conditions	
Power density (W/cm^2)	2.5
Pressure (Pa)	5
Ar/O2 gas content (sccm)	99/1 (1% O$_2$)
Temperature (°C)	650
Substrate distance (cm)	8
Deposition rate (nm/min)	2.5
Targets Composition	
BaTiO$_3$	Nominally undoped
BaTiO$_3$:Mn	0.23 wt% (0.10 at%)
BaTiO$_3$:Nb	0.05 wt% (0.12 at%)
BaTiO$_3$:La	0.50 wt% (0.83 at%)

Substrates were pieces of silicon wafers covered by a platinum layer, which served as a bottom electrode for the electrical experiments and as ground to avoid charging in photoemission measurements. Crystallinity and phase purity were checked by (XRD) analysis, performed at room temperature on a PANalytical (Almelo, The Netherlands) X'pert MPD X'pert MPD-PRO Bragg-Brentano θ-θ geometry diffractometer using Cu K$\alpha_{1,2}$ source. Since the amount of each substituted ion is less than 0.5% and because of line overlap with the major Ba or Ti ions, chemical analysis using Rutherford back scattering was not possible. We thus checked the additional contribution from the substituted heterovalent defects first by X-ray photoelectron spectroscopy (XPS) on single layers on a Physical Electronics PHI 5700 spectrometer at Darmstadt's Integrated System for Material Science (DAISY-MAT) at Technische Universität Darmstadt (TU-Darmstadt), Germany [15]. On this system, we analyzed both in-situ and ex-situ samples. In-situ samples were XPS-probed directly after step-by-step deposition in a sputter deposition chamber connected to the analysis chamber. Ex-situ samples were processed in a sputtering chamber without direct connection to the XPS-chamber. These ex-situ samples were systematically treated prior to XPS measurement by heating to 400 °C in 0.5 Pa of 2 sccm O_2 for 2 h in order to remove adsorbed pollutants. Chemical concentrations were obtained by integrating the peak surface of the main XPS lines (Ba $3d_{5/2}$, Ti 2p, O 1s and Nb 3d) and correcting them with their corresponding atomic sensitivity factors.

X-ray photoelectron spectroscopy was performed using a Physical Electronics PHI 5700 spectrometer (Chanhassen, MA, USA), which is part of the DAISY-MAT. Spectra are excited with monochromated Al Kα radiation and recorded with a takeoff angle of 45°. Binding energies are calibrated daily using the Fermi edge and Ag $3d_{5/2}$ emission of a cleaned Ag foil.

TOF-SIMS depth profiling experiments were performed using 1 keV Cs^+ ions for sputtering and 30 keV Bi^+ for analysis employing a TOF.SIMS 5 (IONTOF, Münster, Germany) at PLACAMAT, Pessac, France.

To measure dielectric permittivity (ε) and losses (tanδ), we sputtered platinum electrodes as 300- and 600-μm-diameter disks on top of 300-nm-thick $BaTiO_3$ layers through a shadow mask as shown in Figure 1. In doing so, we were able to process 18 capacitors on 1×2 cm^2 platinized silicon wafers.
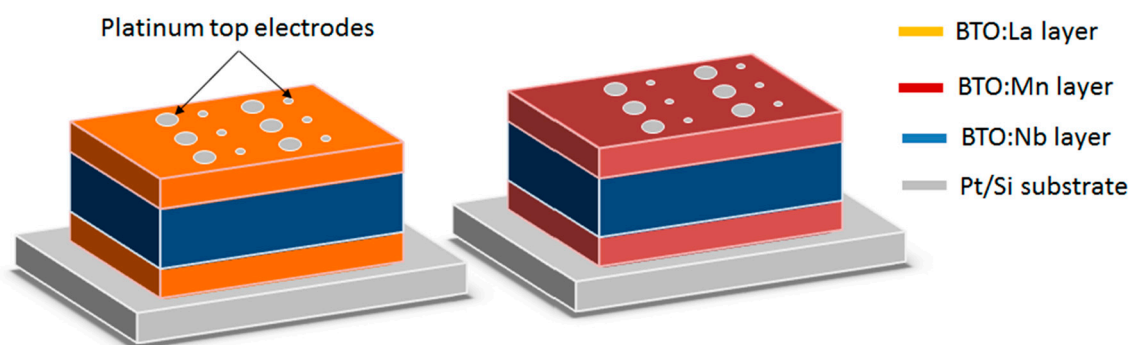

Figure 1. Multilayer structures with Pt top electrodes for electric measurements. Left: LNL10. Right: MNM20.

3. Results and Discussion

The microstructural properties of all thin films have been systematically analyzed by X-ray diffraction (XRD) in θ–2θ mode. XRD patterns of (un)doped single layer films are presented in Figure 2. All films present a polycrystalline perovskite structure without a preferential orientation or secondary phases in the detection limit of the probing technique. We did not find any significant shift nor preferential orientations with the insertion of dopants nor with the introduction of stacks (heterostructures). The overall chemical content and microstructure of the films is thus following our previous reports on similar systems [12,13].
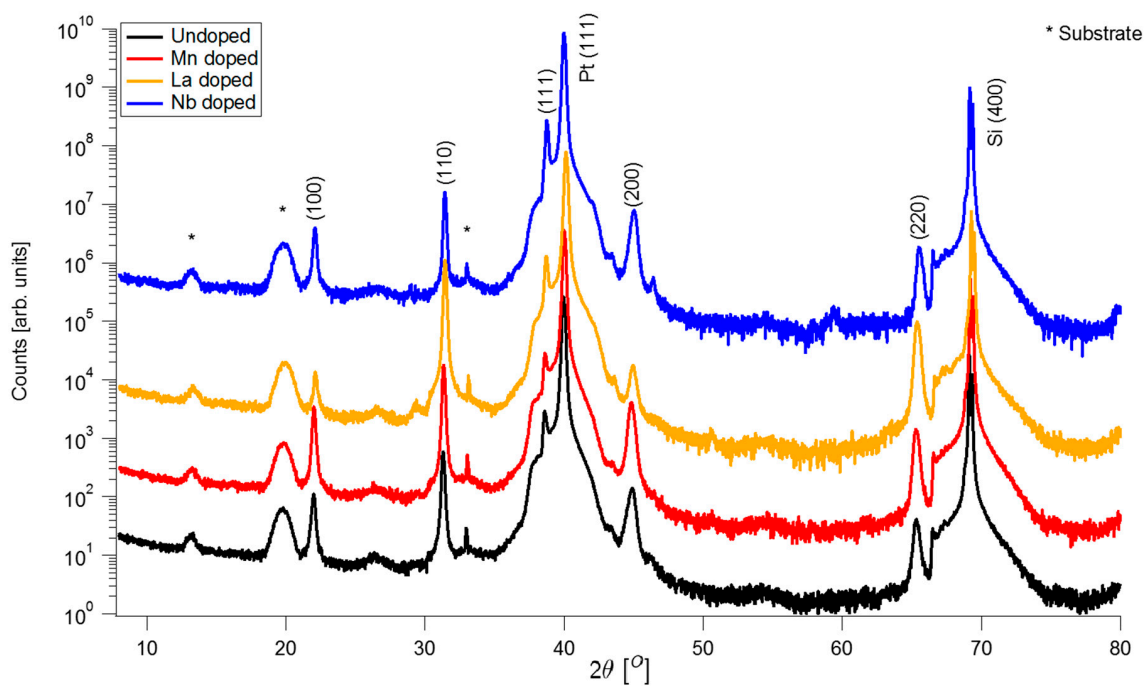
Figure 2. XRD diffraction patterns (2 theta) of (un)doped samples.

The dielectric permittivity (ε) and losses (tanδ) at 100 kHz and room temperature (RT) of undoped, Mn-, La-, Nb-doped BaTiO$_3$ films and heterostructures are reported in Table 2.

Table 2. Relative permittivity and dielectric losses values are shown for 100 kHz, 0 V and room temperature. XPS results are in situ E_F (Fermi level position) —E_{VBM} (valence band maximum) (eV) values for single doped films and ex situ E_F-E_{VBM} values for heterostructures. The abbreviations indicate tri-layer structures where M, N, and L correspond to Mn, Nb and La, respectively.

Single Doped Films			
Sample	ε	tan (δ) (%)	XPS (eV)
Undoped	110	1.5	2.7
Mn doped	250	1.1	2.2
La doped	400	2.2	2.8
Nb doped	640	2.0	2.8
Heterostructures			
Sample	ε	tan (δ) (%)	XPS (eV)
MNM20	400	1.3	2.2
MNM10	530	2.2	2.2
MNM5	850	5.0	2.4
NMN20	440	2.5	2.1
LNL10	1100	3.1	2.3
NLN10	540	2.3	2.3

Dielectric permittivity and losses of undoped, Mn and La doped samples are comparable to those of other sputtered BaTiO$_3$ films on Si/Pt substrates [12,16]. Nb doping induces a very large increase in ε due to electron charges generated by Nb^{5+}/Ti^{4+} substitution, along with a well-defined band bending at the Pt electrode interfaces, as evidenced by XPS [17]. The interfacial space charge at the electrodes

may also increase the effective dielectric permittivity as reported for BaTiO$_3$ single crystals [18]. However, with Pt-electrode/oxide interfaces being hardly controlled, we decided to investigate internal interfaces generated by stacking several differently doped (Mn, La, Nb) BaTiO$_3$ films.

The prepared multilayer heterostructures consist mostly of one core layer embedded between two similar thin layers, keeping the total thickness at about 300 nm. In our notation, M, L, N stand for manganese-, lanthanum- and niobium-doped films, respectively, and the number following a given stack is the outer layer thickness. For example, MNM20 means a stack of a 260-nm-thick Nb-doped BaTiO$_3$ film between two 20-nm Mn-doped layers. In a similar way as for single layers, we measured the dielectric permittivity and losses over 18 MIM capacitors on a single substrate. We also repeated the full process several times to confirm its reproducibility. RT dielectric parameters of several multilayers are reported in Table 2. A large increase in dielectric permittivity along with reasonably low losses was most pronounced for the LNL stacks (see Figure 3). The dielectric permittivity was mostly independent of temperature above 150 K, ruling out ferroelectric behavior, and was mostly independent of frequency (100Hz to 1MHz) at RT (see Figure 4). The absence of ferroelectric phase transition is common for sputtered polycrystalline BaTiO$_3$ thin films [12,14,16,17,19]. It was also obvious that the dielectric permittivity of the stack was much higher than that of a series capacitor circuit modeling the 3 capacitive layers. This was a first evidence of an interfacial contribution to the dielectric permittivity of the stack.
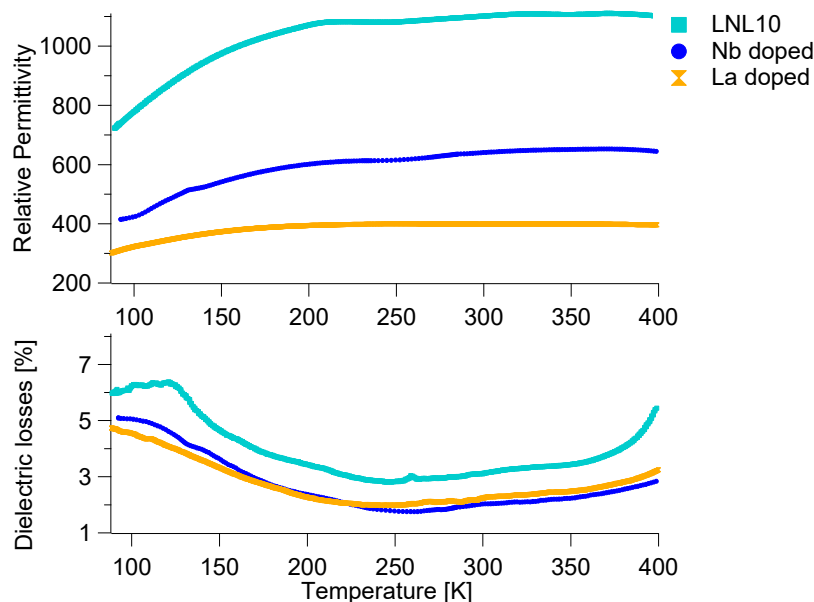

Figure 3. Temperature dependence of the relative permittivity and dielectric losses at 100 kHz of Nb- and La-doped BaTiO$_3$ films and of an LNL10 multilayer structure.

To confirm this, we have analyzed the electronic structure of our films by XPS. First, a survey spectrum was used to identify the chemical elements present at the surface including possible contaminations. Second, we performed a high resolution measurement of the core levels of each element on their most intense peaks, in our case Ba 3d$_{5/2}$, Ti 2p, O 1s and Ba 4d, in order to analyze oxidation states, surface composition and electronic structure. Finally, a detailed spectrum of the valence band was recorded, as the position of the valence band edge indicates the position of Fermi level, indicating the electrical nature of our semiconducting films given the known value (3.2 eV) of the bandgap [20]. Figure 5 shows a typical in-situ XPS routine analysis of an undoped BaTiO$_3$ thin film.

In addition to this, E$_F$-E$_{VB}$ can be obtained by measuring the core level binding energy E$_{CL}$ of any BaTiO$_3$ core level as the difference E$_{VB}$-E$_{CL}$ is a material constant. In this work, the value for E$_{VB}$-E$_{CL}$ was determined by XPS in-situ measurements of the binding energies of the core levels Ba 3d, O 1s, Ti 2p and Ba 4d of several doped and undoped BaTiO$_3$ thin films.
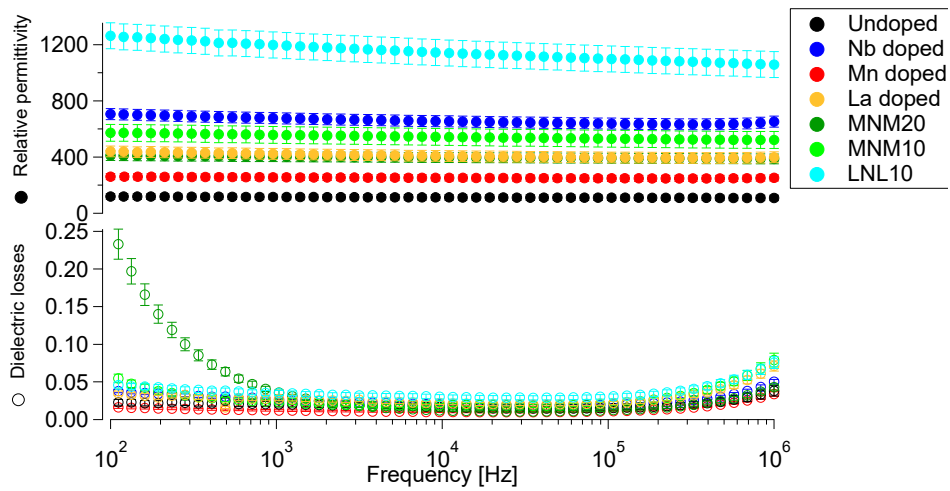
Figure 4. Dielectric permittivity and dielectric losses vs. frequency (V_{osc} = 0.01 V) of (un)doped samples and different multilayer heterostructures at 293 K.

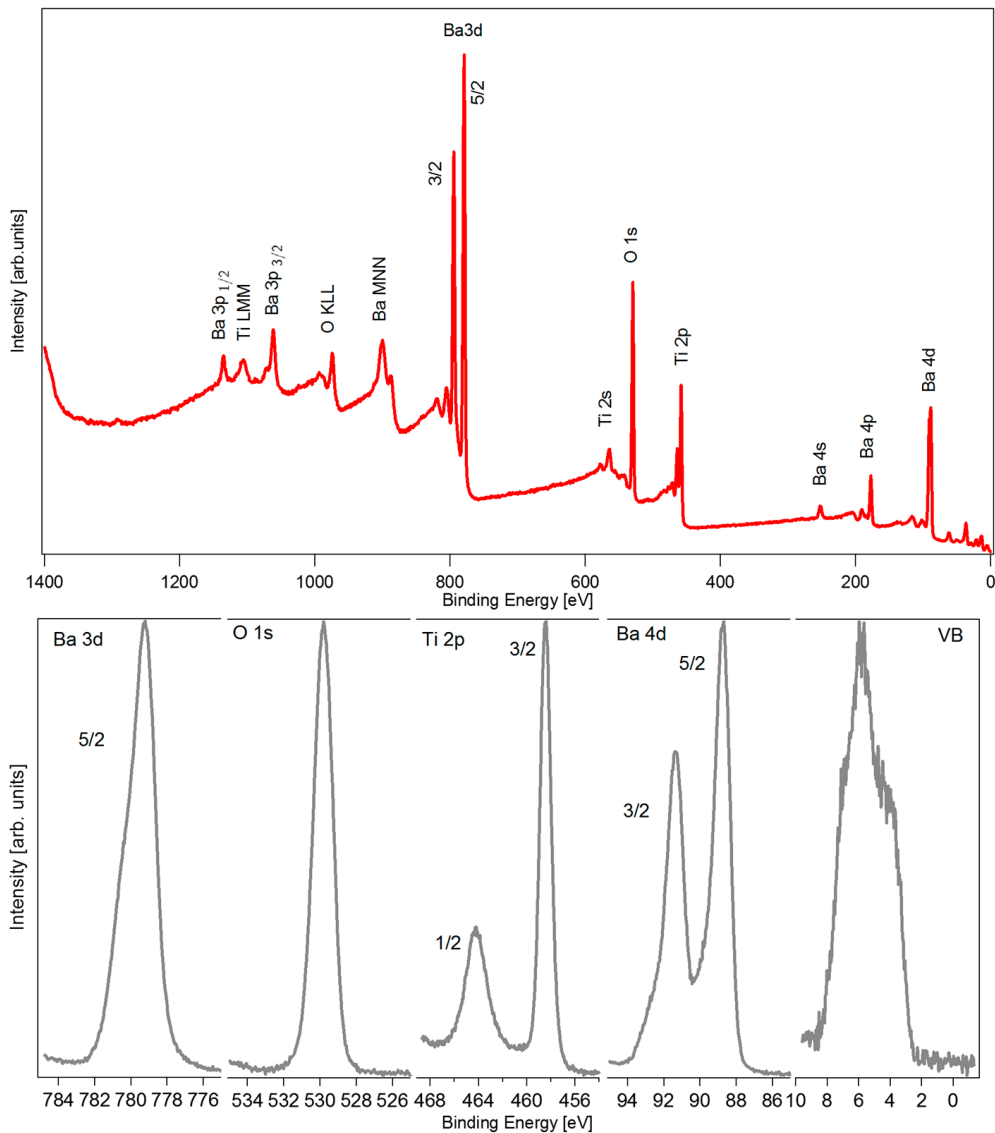**Figure 5.** XPS survey (**top**) and core-levels and valence bands (VB) (**bottom**) of an undoped $BaTiO_3$ thin film recorded with monochromatized Al K_α radiation.

The low concentration of dopants made their detection by XPS difficult. The presence of La and Mn could not be confirmed, and only Nb XPS main line ($3d_{5/2}$) showed up clearly, demonstrating that the Nb concentration was well above the XPS detection limit of about 0.1 at%. The presence of La and Mn was confirmed by TOF-SIMS. Doping $BaTiO_3$ with donor dopants such as Nb and La should raise the Fermi level position closer to the conduction band [21,22]. This is indeed observed from the XPS binding energies of in-situ deposited layers. Nb-doped and La-doped films both show E_F-E_{VB} = 2.7 ± 0.1 eV and E_F-E_{VB} = 2.7 ± 0.1 eV, close to previous work 2.73 eV [12], while Mn-doped $BaTiO_3$ thin films display E_F-E_{VBM} = 2.2 ± 0.1 eV.

As several samples have been prepared outside DAISY-MAT, it is relevant to indicate the differences between ex-situ and in-situ samples. In Figure 6 we compare the Fermi energies of several $BaTiO_3$ thin films, including the sample prepared at ICMCB (ex-situ) and those prepared at DAISY-MAT (in-situ).
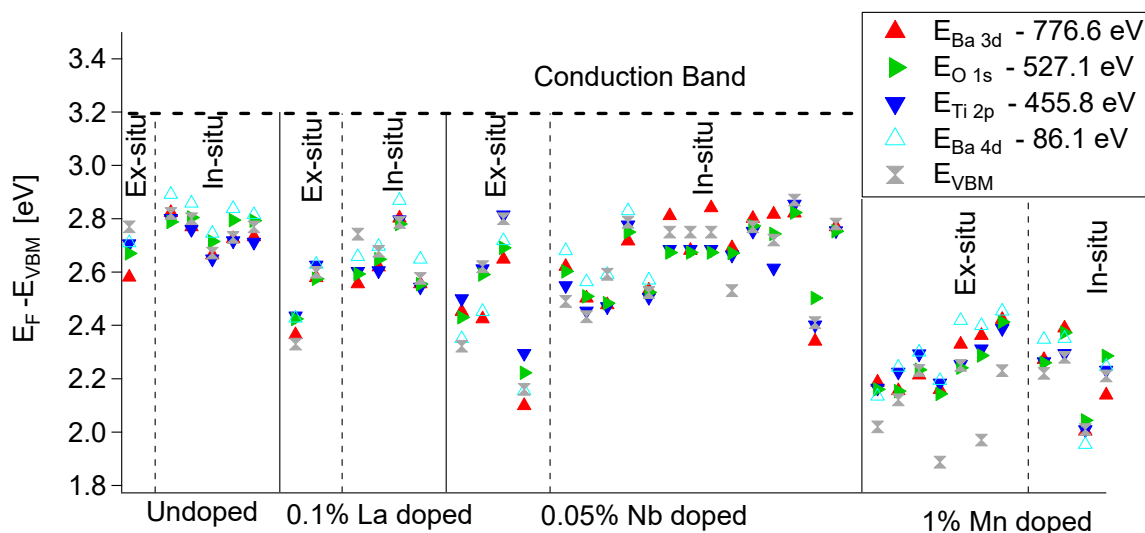

Figure 6. Fermi level position of differently doped BaTiO3 thin samples analyzed directly after deposition without breaking vacuum (in-situ) or after deposition in a disconnected deposition chamber after surface cleaning by annealing in a low-pressure oxygen environment (ex-situ).

The Fermi energies extracted from the core levels of the in-situ films are within 0.05 eV from the direct determination using the valence band maximum extrapolation [23] whereas the ex-situ films exhibit a larger scattering of 0.12 eV. This larger scattering of the ex-situ films may originate from a potential surface modification due to the cleaning procedure prior to the measurement. A Fermi level close to the conduction band results in a higher concentration of free electrons and, therefore, to a higher conductivity. In undoped films, the microstructure has a larger effect on the conductivity, as the columnar structure will increase the leakage currents compared to ceramics or single crystals. For the undoped samples, the E_F is far from the conventional understanding of an insulator, that is to say, a mid-gap Fermi level position (1.6 eV above E_{VBM}). This could be explained by the oxygen-poor atmosphere during deposition, creating a high concentration of oxygen vacancies that are compensated electronically, raising the E_F closer to the conduction band. For the Mn-doped sample, E_F obtained in this work is in accordance with the value found in the literature for the impurity transition level of $Mn^{2+/3+}$ [24,25]. It is worth mentioning that due to the deposition conditions, we should be able to reach the second transition level, $Mn^{3+/4+}$, by oxidizing treatments. The decrease in the Fermi level position within the band gap under Mn doping is consistent with previous reports on sol–gel films [16].

To confirm an interfacial contribution to the dielectric properties of the LNL heterostructure, we investigated the electronic structure of the interface between La-doped and Nb-doped $BaTiO_3$ films by in situ XPS [26]. The evolution of the Fermi level with respect to the valence band maximum (E_F-E_{VB}) was followed during a step-by-step deposition of either an La-doped on an Nb-doped layer (Figure 7, top left) or vice versa (Figure 7, top right). After each deposition step, the value E_F-E_{VB} was obtained

by measuring both the leading edge of the valence band maximum and the core level binding energy of any BaTiO$_3$ core level (Ba 3d$_{5/2}$, O 1s, Ti 2p) (Kraut method) [27]. The experiment was conducted in several steps: (i) a 10-nm-thick La-doped layer was deposited onto the Si/Pt substrate; (ii) for studying the deposition induced changes, a stepwise deposition of an Nb-doped layer was performed until a thickness of 20 nm was reached; (iii) an Nb-doped layer of 260 nm was deposited to complete the total thickness of the Nb-doped layer of 280 nm; (iv) an La-doped layer was stepwise deposited until a thickness of 10 nm to follow the effect on the interface. The sequence of the experiment is shown in Figure 7 at the top from right to left.
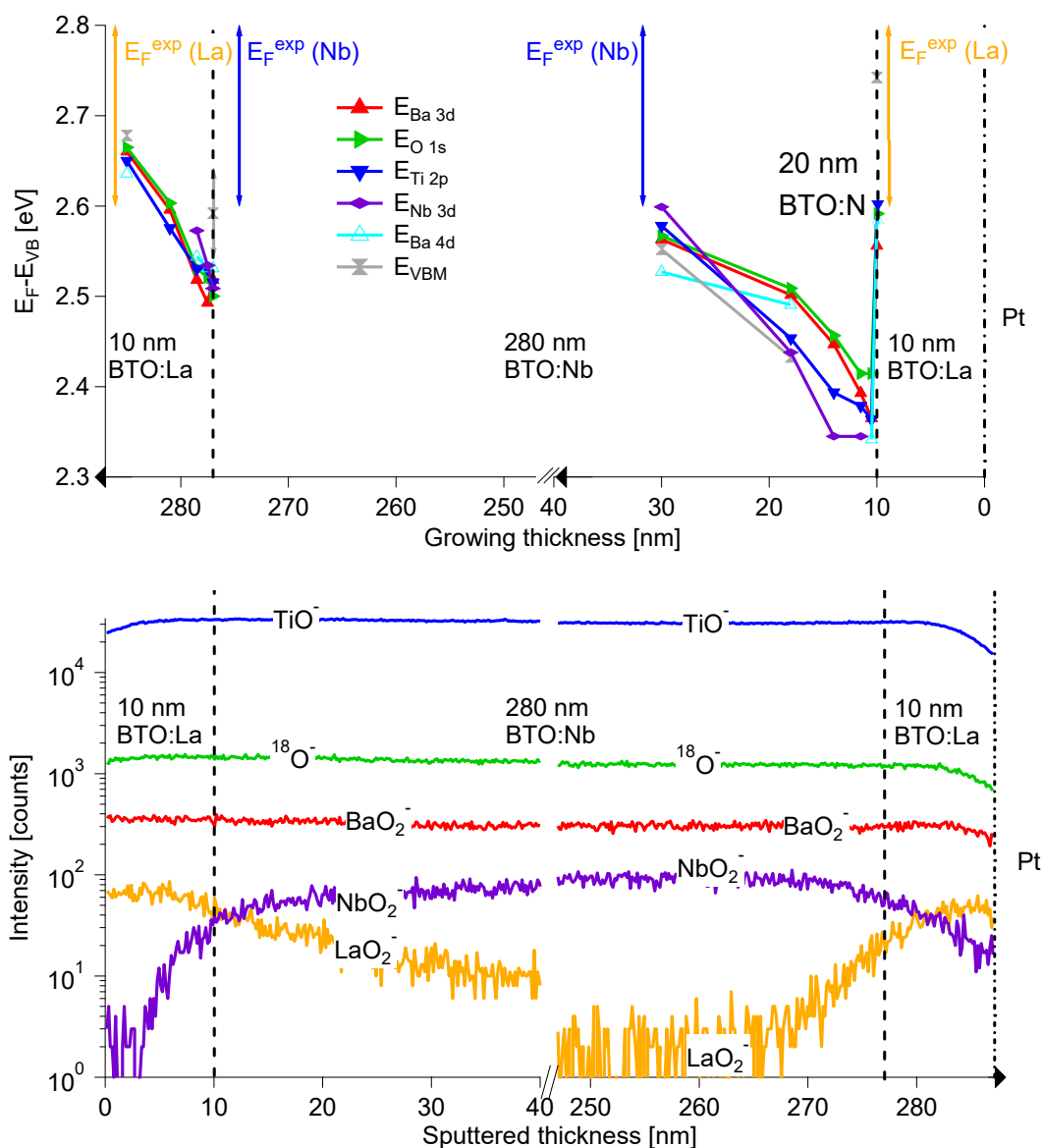

Figure 7. Top. In situ XPS stepwise interface experiments of 8 nm thick BTO:La layer on a BTO:Nb layer (left) and a 20-nm-thick BTO:Nb layer on a BTO:La substrate (right). First points (starting from dashed lines) correspond to a single doped layer. For reference, the range of Fermi level positions with respect to the valence band of single doped films obtained by XPS in situ is plotted. As E$_{CL}$-E$_{VBM}$ is a material constant, the values of core level positions of each element were obtained by subtracting: 776.57 eV for Ba3d, 527.09 eV for O1s, 455.79 eV for Ti2p, 204.40 eV for Nb3d and 86.07 eV for Ba4d (values obtained by averaging over 100 samples). Error on these values is ±0.05 eV. Bottom. Time-of-flight secondary ion mass spectroscopy (TOF-SIMS) depth profiling of sample LNL10. Analyzed ion species are written over their corresponding lines.

A sharp immediate drop in Fermi level (0.25 eV) and a consecutive variation of band position over about 20 nm was observed during deposition of the Nb-doped layer onto La-doped substrate (right), whereas less pronounced effects (0.1 eV, 8 nm) were observed for the reverse deposition (left). The sharp drop in Fermi level after the initial deposition of Nb-doped BTO onto the La-doped substrate was not expected, as donor type dopants were present in both films. However, it was observed that the abrupt lowering of E_F is associated with an unexpectedly high Nb intensity in the XPS spectra, which suggests an enhanced Nb concentration at this interface. This might be the origin for the depletion layer and the enhanced permittivity. Nb is a donor in BTO and lightly doped polycrystalline bulk ceramics show resistivities of 10 Ωcm and a pronounced positive temperature coefficient of resistivity (PTCR) [7,28,29]. When the Nb concentration is increased above 0.1 wt%, the samples become insulating again. This behavior is likely related to insulating grain boundaries, which are probably induced by segregation of Ba vacancies or Nb donors to the grain boundary core. It is not expected that the grains themselves become insulating with an increasing donor concentration.

TOF-SIMS is a very efficient way to qualitatively assess the presence of dopants in individual layers as well as their interdiffusion at interfaces in multilayers. Using TOF-SIMS, we could confirm that the three types of dopants were indeed present in every individual layers and that the Nb concentration is enhanced near the bottom interface. In order to obtain further insight into interface chemistry, TOF-SIMS depth profiling experiments were performed on the LNL10 heterostructure using 1 keV Cs^+ for sputtering and 30 keV Bi^+ for analysis. Whereas XPS experiments were performed during the growth, TOF-SIMS was performed ex situ on the same sample in reverse order by depth profiling. The evolution of intensities with sputter time is given from left to right in Figure 7.

Starting from the top of the heterostructure, the interface from the La-doped layer towards the Nb-doped one is as sharp as expected from the depth resolution of TOF-SIMS [30]. Meanwhile, the Nb signal is very small in the La-doped layer, which shows that interdiffusion of dopants did not occur. This is slightly different for the bottom interface close to the Si/Pt substrate. The intensity of the Gaussian-like LaO_2^- peak remains below that of the outer La-doped layer, whereas the intensity of the NbO_2^- peak does not decay as fast as expected without interdiffusion (=$I_{max}/3$ in the middle of the layer). Long range interdiffusion between the dopant ions was thus much more efficient at the bottom Nb/La interface as compared to the top La/Nb one. In agreement with the XPS analysis, the Nb content near the bottom interface was also larger than at the top contact.

Such interface contrast between bottom and top interfaces has been observed by in-situ XPS in metal/ferroelectric/metal structures and explained in terms of a different thermal budget [31]. The bottom interface was exposed to the growth temperature of 650 °C for several hours, while the top interface was only exposed for a few minutes. We therefore ascribed the strong disparity in the La/Nb/La heterostructures to the thermal history of the sample. What is new here, and obviously not observed in metal/ferroelectric interfaces, is that cross diffusion of dopants through oxide/oxide interfaces is possible because of the crystalline continuity at the interface and column-like grains. This is why we linked the specific band bending at the bottom Nb/La interface observed by in-situ XPS to the interdiffusion observed by TOF-SIMS.

For all other investigated interfaces, the band bending was much smoother and the interdiffusion between layers much more limited, leading to a moderate increase in dielectric permittivity in NLN and NMN cases.

We summarize band bending and diffusion length of the different cations in LNL heterostructure capacitor in Figure 8. Band bending and barrier heights at the Pt electrode interfaces were derived from the results of a previous study [17].
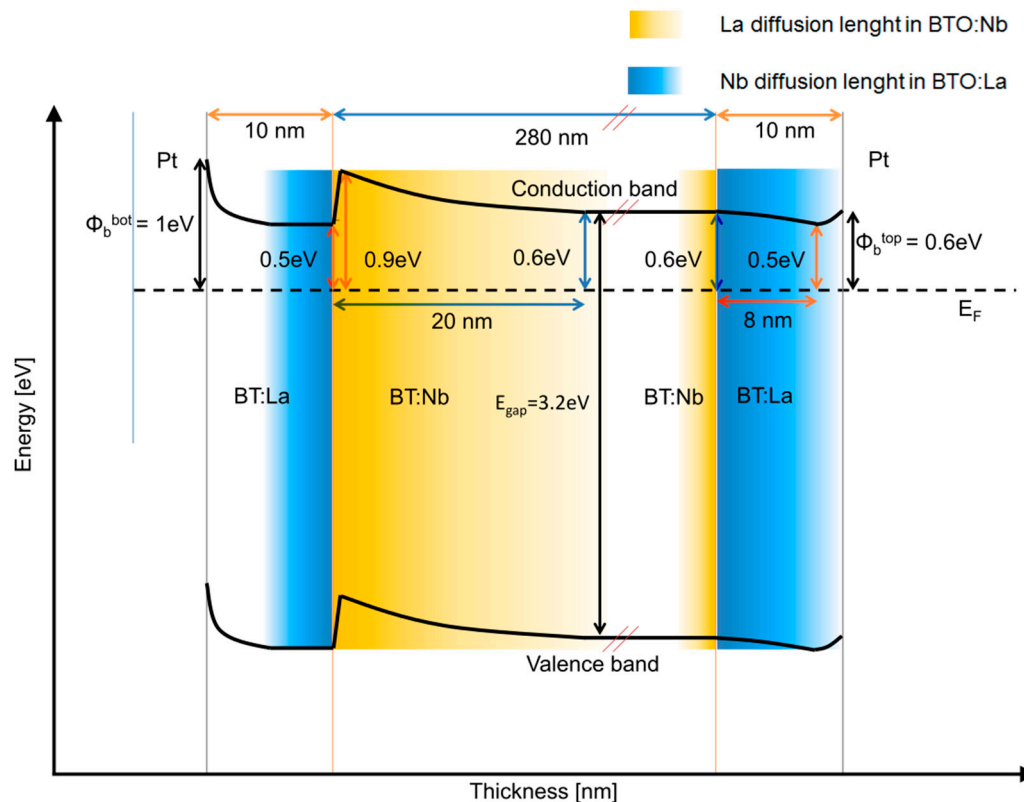
Figure 8. Band diagram of capacitor LNL10 with Pt barrier heights derived from the results of E. Arveux [17].

4. Conclusions

To summarize, we have achieved large and temperature-stable dielectric permittivity by a three-layer stack of La-doped and Nb-doped $BaTiO_3$ thin films. Using XPS, we could link these features to interface localization of space charges resulting in large band bending over more than a thickness of 10 nm (see Figure 7). TOF-SIMS experiments suggest that this band bending results from cross diffusion of dopants at the interface. Such layered structures may be useful to model so-called giant permittivity in isotropic polycrystalline samples.

References

1. Sigman, J.; Brennecka, G.L.; Clem, P.G.; Tuttle, B.A. Fabrication of perovskite-based high-value integrated capacitors by chemical solution deposition. *J. Am. Ceram. Soc.* **2008**, *91*, 1851–1857. [CrossRef]
2. Dietz, G.W.; Schumacher, M.; Waser, R. Leakage currents in Ba 0.7 Sr 0.3 TiO3 thin films for ultrahigh-density dynamic random access memories dynamic random access memories. *J. Appl. Phys.* **2014**, *82*, 2359. [CrossRef]

3. Lemée, N.; Dubourdieu, C.; Delabouglise, G.; Sénateur, J.P.; Laroudie, F. Semiconductive Nb-doped BaTiO3 films grown by pulsed injection metalorganic chemical vapor deposition. *J. Cryst. Growth* **2002**, *235*, 347–351. [CrossRef]

4. Dubourdieu, C.; Bruley, J.; Arruda, T.M.; Posadas, A.; Jordan-Sweet, J.; Frank, M.M.; Cartier, E.; Frank, D.J.; Kalinin, S.V.; Demkov, A.A.; et al. Switching of ferroelectric polarization in epitaxial BaTiO 3 films on silicon without a conducting bottom electrode. *Nat. Nanotechnol.* **2013**, *8*, 748–754. [CrossRef]

5. Tabata, H.; Tanaka, H.; Kawai, T. Formation of artificial BaTiO$_3$/SrTiO$_3$ superlattices using pulsed laser deposition and their dielectric properties. *Appl. Phys. Lett.* **2006**, *1970*, 1998–2001.

6. Horwitz, J.S.; Chang, W.; Kim, W.; Qadri, S.B.; Pond, J.M.; Kirchoefer, S.W.; Chrisey, D.B. The effect of stress on the microwave dielectric properties of BaO$_5$ SrO$_5$ TiO$_3$ thin films. *J. Electron.* **2000**, *3*, 357–363.

7. Heywang, W. Semiconducting barium titanate. *J. Mater. Sci.* **1971**, *6*, 1214–1224. [CrossRef]

8. Ramirez, A.P.; Subramanian, M.A.; Gardel, M.; Blumberg, G.; Li, D.; Vogt, T.; Shapiro, S.M. Giant dielectric constant response in a copper-titanate. *Solid State Commun.* **2000**, *115*, 217–220. [CrossRef]

9. Ikeda, N.; Ohsumi, H.; Ohwada, K.; Ishii, K.; Inami, T.; Kakurai, K.; Murakami, Y.; Yoshii, K.; Mori, S.; Horibe, Y.; et al. Ferroelectricity from iron valence ordering in the charge-frustrated system LuFe$_2$O$_4$. *Nature* **2005**, *436*, 1136–1138. [CrossRef]

10. Wu, J.; Nan, C.W.; Lin, Y.; Deng, Y. Giant dielectric permittivity observed in Li and Ti doped NiO. *Phys. Rev. Lett.* **2002**, *89*, 1–4. [CrossRef]

11. Popovic, Z.V.; Stolz, H.J. Infrared and raman spectra of germanium dichalcogenides I. GeS$_2$. *Phys. Stat. Solid. B* **1981**, *106*, 337–348. [CrossRef]

12. Arveux, E.; Payan, S.; Maglione, M.; Klein, A. Applied Surface Science Surface segregation in Nb-doped BaTiO$_3$ films. *Appl. Surf. Sci.* **2010**, *256*, 6228–6232. [CrossRef]

13. Reymond, V. Nouvelles Couches Minces et Multicouches Dérivées de Batio$_3$: Optimisation des Propriétés Diélectriques. Ph.D. Thesis, Université de Bordeaux, Bordeaux, France, 2004.

14. Simon, Q.; Daumont, C.J.M.; Payan, S.; Gardes, P.; Poveda, P.; Wolfman, J.; Maglione, M. Extreme dielectric non-linearities at the convergence point in Ba1-xCaxTi1-xZrxO$_3$ thin films. *J. Alloys Compd.* **2018**, *747*, 366–373. [CrossRef]

15. Klein, A. Interface properties of dielectric oxides. *J. Am. Ceram. Soc.* **2016**, *99*, 369–387. [CrossRef]

16. Levasseur, D. Nouvelle Génération de Capacités Intégrées: Influence des Matériaux sur les Performances Diélectriques des Capacités en Couches Minces. Ph.D. Thesis, Université de Bordeaux, Bordeaux, France, 2015.

17. Arveux, E. Propriétés de Surfaces et Interfaces de Couches Minces Ferroélectriques de BaTiO$_3$ Étudiées par Spectroscopie de Photoémission in-situ. Ph.D. Thesis, Université de Bordeaux, Bordeaux, France, 2009.

18. Maglione, M.; Belkaoumi, M. Electron-relaxation-mode interaction in Ba Ti0$_3$: Nb. *Phys. Rev. B* **1992**, *45*, 2029–2034. [CrossRef]

19. Reymond, V.; Payan, S.; Michau, D.; Manaud, J.; Maglione, M. Structural and electrical properties of BaTi$_{1-x}$Zr$_x$O$_3$ sputtered thin films: Effect of the sputtering conditions. *Thin Solid Films* **2004**, *467*, 54–58. [CrossRef]

20. van Benthem, K.; Elsässer, C.; French, R.H. Bulk electronic structure of experiment and theory. *J. Appl. Phys.* **2011**, *90*, 6156. [CrossRef]

21. Chan, H.M.; Harmer, M.P.; Smyth, D.M. Compensating defects in highly donor-doped BaTiO$_3$. *J. Am. Ceram. Soc.* **1986**, *10*, 507–510. [CrossRef]

22. Morrison, F.D.; Coats, A.M.; Sinclair, D.C.; West, A.R. Charge compensation mechanisms in La-doped BaTiO$_3$. *J. Electroceramics* **2001**, *6*, 219–232. [CrossRef]

23. Chambers, S.A.; Droubay, T.; Kaspar, T.C.; Gutowski, M.; Van Schilfgaarde, M. Accurate valence band maximum determination for SrTiO$_3$(0 0 1). *Surf. Sci.* **2004**, *554*, 81–89. [CrossRef]

24. Moretti, P.; Michel-Calendini, F.M. Impurity energy levels and stability of CR and MN ions in cubic batio3. *Phys. Rev. B* **1987**, *36*, 3522–3527. [CrossRef] [PubMed]

25. Wechsler, B.A.; Klein, M.B. Thermodynamic point defect model of barium titanate and application to the photorefractive effect. *J. Opt. Soc. Am. B* **1988**, *5*, 1711. [CrossRef]

26. Klein, A. Energy band alignment at interfaces of semiconducting oxides: A review of experimental determination using photoelectron spectroscopy and comparison with theoretical predictions by the electron affinity rule, charge neutrality levels, and the common anion. *Thin Solid Films* **2012**, *520*, 3721–3728. [CrossRef]

27. Kraut, E.A.; Grant, R.W.; Waldrop, J.R.; Kowalski, S.P. Precise determination of the Valence-Band Edge in X-ray Photoemission spectra: Application to measurement of semiconductor interface potentials. *Phys. Rev. Lett.* **1980**, *44*, 1620–1623. [CrossRef]

28. Slipenyuk, A.M.; Glinchuk, M.D.; Laguta, V.V.; Bykov, I.P.; Bilous, A.G.; V'yunov, O.I. Impurity and intrinsic defects in barium titanate ceramics and their influence on PTCR effect. *Ferroelectrics* **2003**, *288*, 243–251. [CrossRef]

29. Lewis, G.V.; Catlow, C.R.A. PTCR Effect in BaTiO$_3$. *J. Am. Ceram. Soc.* **1985**, *58*, 555–558. [CrossRef]

30. Hofmann, S.; Liu, Y.; Jian, W.; Kang, H.L.; Wang, J.Y. Depth resolution in sputter profiling revisited. *Surf. Interface Anal.* **2016**, *48*, 1354–1369. [CrossRef]

31. Schafranek, R.; Payan, S.; Maglione, M.; Klein, A. Barrier height at (Ba, Sr) TiO$_3$/Pt interfaces studied by photoemission. *Phys. Rev. B* **2008**, 30–33. [CrossRef]